Fermi-surface topology of the heavy-fermion antiferromagnetic superconductor $CeIn_3$

M. Biasini* and G. Ferro
ENEA, Via Don Fiammelli 2, 40129 Bologna, Italy

A. Czopnik
Trzebiatowski Institute of Low Temperature and Structure Research, P.O. Box 937 Wroclaw, Poland.
(Received 27 May 2003; published 23 September 2003)

A three-dimensional mapping of the Fermi surface (FS) of the heavy-fermion antiferromagnetic system $CeIn_3$ in the paramagnetic phase was determined via measurements of the angular correlation of the electron-positron annihilation radiation for five crystal orientations. The two equivolume FS sheets observed agree with the predictions of our band-structure calculations regarding the Ce $4f$ electrons as fully localized. Moreover, a comparison of our results with the de Haas–van Alphen signals observed in the antiferromagnetic phase suggests that the f electrons retain the local atomic character in the magnetically ordered phase.

DOI: 10.1103/PhysRevB.68.094513 PACS number(s): 74.70.Tx, 71.18.+y, 71.27.+a, 71.60.+z

I. INTRODUCTION

The interplay of heavy fermion behavior, magnetic ordering, and superconductivity (s.c.) under application of pressure, which was observed recently in some rare-earth-based compounds, has arisen increased and widespread interest.[1] It is well known that, since several heavy-fermion systems are located on the brink between a paramagnetic, Kondo-like, and a magnetically ordered, Ruderman-Kittel-Kasuya-Yosida (RKKY)-like, ground state, one can in many cases switch from one to another behavior by tuning the lattice constant under alloying [see, for example, the system $Ce(Cu_xAu_{1-x})_6$, Ref. 2] or (conversely) under application of pressure.[2] On the other hand, one can find a large class of heavy fermions (CeB_6 being the archetype example) where the magnetically ordered ground state coexists with the heavy-fermion behavior. These are the systems which have displayed the fascinating interaction between the often considered antagonist phenomena of superconductivity and (anti)ferromagnetism. Indeed, the fact that superconductivity in $CePd_2Si_2$, $CeRh_2Si_2$, UGe_2, $CeIn_3$ is observed in a thin shell of pressure, just about the point of disappearance of magnetic order, and not at higher pressures, suggests that these two phenomena are intimately related.[1] However, the role played by the electrons carrying the magnetic moments to the onset of s.c. (direct contribution to the formation of the Cooper pairs or other) has not been clarified. Whereas the majority of these systems have a rather complex structure, tetragonal or orthorhombic, with few nonequivalent atoms per primitive cell, $CeIn_3$, crystallizing in the simple cubic $AuCu_3$-type structure, constitutes a unique case for studying these phenomena. Its Sommerfeld cofficient and Néel temperature T_N (at atmospheric pressure) are 130 mJ/K^2 mol and 10.1 K, respectively. At ambient pressure $CeIn_3$ orders in a simple (type II) magnetic structure where the Ce moments are aligned antiferromagnetically in adjacent (111) ferromagnetic planes. The FS of the antiferromagnetic (AF) phase was investigated experimentally via de Haas–van Alphen (dHvA) experiments.[3–5] The angular dependence of the dHvA frequency branches observed in $CeIn_3$ differed from those observed for the isostructural non-f-electron compound $LaIn_3$. However, since the results were not compared to a band-structure calculation, it was not established whether these differences were due to itinerancy of the f electrons or to the influence of the magnetic Brillouin zone (BZ) boundaries of $CeIn_3$. More recently, the electronic structure of AF $CeIn_3$ was studied theoretically.[6] The calculation, including the f electrons in the valence bands, yielded a magnetic hyperfine field at the Ce site in reasonable agreement with the experimental value.[6] However, the resulting total (spin plus orbital) magnetic moment (0.177 μ_B) was much smaller than the experimental value of 0.65 μ_B.[7] Moreover, the band structure of paramagnetic $CeIn_3$ with the Ce $4f$ electrons regarded as corelike states was calculated by Kioussis *et al.*[8] However, up to now, no experimental or theoretical determination of the Fermi surface (FS) in the paramagnetic phase has been attempted. The two-dimensional angular correlation of the electron-positron annihilation radiation (2D-ACAR) experiment, which can be performed above T_N, is suitable to this purpose. Moreover, this technique has the ability to sample the BZ of truly three-dimensional systems in a Cartesian mesh providing unique experimental images of the FS.[9–11]

In detail, by measuring the distribution $N(\theta_x, \theta_y)$ of the deviation angles from anticollinearity of the annihilation γ rays, the experiment determines a two-dimensional (2D) projection of the 3D electron-positron (ep) momentum density, $\rho^{ep}(\boldsymbol{p})$.[12] The contribution to $\rho^{ep}(\boldsymbol{p})$ from the conduction bands l is discontinuous at points $\boldsymbol{p}_{F_l}=(\boldsymbol{k}_{F_l}+\boldsymbol{G})$, where $\boldsymbol{G}$ is a reciprocal lattice vector and $\boldsymbol{k}_{F_l}$ are the reduced Fermi wave vectors in the first BZ. The standard Lock-Crisp-West (LCW) transformation,[13] extensively used in the data analysis of the 2D-ACAR spectra, reinforces these discontinuities by folding the momentum distribution $\rho^{ep}(\boldsymbol{p})$ back onto the first BZ by translation over the appropriate vectors $\boldsymbol{G}$. If the summation is performed over a sufficient portion of momentum space the result is[14]

$$\rho^{ep}_{LCW}(\boldsymbol{k})=\sum_n \theta(E_F-\epsilon_{\boldsymbol{k},n}) \int |\psi^n_{\boldsymbol{k}}(\boldsymbol{r})|^2 \, |\phi(r)|^2 \, g^n_{\boldsymbol{k}}(\boldsymbol{r})\, d\boldsymbol{r}. \quad (1)$$

Here ϕ denotes the positron wave function, $\epsilon_{k,n}$ is the energy eigenvalue of the electron from band n with Bloch wave vector $\boldsymbol{k}$ and wave function $\psi_{\boldsymbol{k}}^{n}$. The factor $g_{\boldsymbol{k}}^{n}(\boldsymbol{r})$ accounts for the ep correlations.[15] In general, although the mapping of the FS is facilitated when the overlap integral in Eq. (1) is a weakly varying function of $\boldsymbol{k}$, the FS discontinuities [marked by the step function of Eq. (1)] are not shifted by this $\boldsymbol{k}$ dependence. Actually, prior to applying the 3D LCW transformation it is necessary to reconstruct tomographically the 3D $\rho^{ep}(\boldsymbol{p})$ on the base of its 2D projections.

In this work, we provide a topological description of the FS sheets of $CeIn_3$. The results are compared to *ab initio* band-structure calculations produced by the code WIEN97,[16] adopting the full potential linearized augmented plane-wave (FLAPW) method within the local-density approximation (LDA). Finally, from our estimates of the FS we simulate the angular dependence of dHvA frequencies, suggest an interpretation of the dHvA experiment, and discuss these results in relation to the AF-superconductive transition.

II. EXPERIMENTAL PROCEDURES AND DETAILS OF THE CALCULATIONS

The crystal structure of $CeIn_3$ is the cubic $L1_2$ (space group *Pm3m*), with lattice constant $a=4.69$ Å. The 2D-ACAR experiments were performed on single crystals grown according to the procedure described in Ref. 9. The 2D-ACAR experiments were carried out with a setup based on a pair of Anger cameras, described in detail in Ref. 17. The five projections collected had integration directions (perpendicular to the $\boldsymbol{p}_z \equiv [001]$ axis) spanning uniformly the angle comprised between the [100] and the [110] axes. Each spectrum, acquired at the temperature of 60 K in a vacuum of 1×10^{-6} torr accumulated $\approx 3\times10^{8}$ raw coincidence counts in a (288×288) matrix with a bin size of (0.02×0.02) a.u.^{2}. The estimated overall experimental resolution was equivalent to $\approx$14% of the BZ size. The spectra were subjected to the usual correction procedures and deconvoluted according to the Van Citter–Gerhardt algorithm.[9] The electron-positron momentum densities were reconstructed via the Cormack's[18] and modified filtered-back-projection (FBP) (Ref. 19) algorithms. Finally, the 3D-LCW (Ref. 13) transformation was applied. Further details of the data analysis can be found in Ref. 9. The total amplitude variation of the resulting 3D-LCW densities provided by both reconstruction methods (Cormack, FBP), showing very similar features, was 16%.

The band structure was calculated treating the $4f$ electrons either as ordinary band electrons (f band) or as core like states (f core). In the interstitial region, the plane waves expansion was truncated at the maximum wave vector $K_{max}=2.7$ a.u. Inside the muffin tin (MT) spheres (having MT radii $R=3$a.u.) we used spherical harmonics with angular momenta up to $l_{max}=10$ for the potential, the charge density, and the wave functions. The irreducible part of the BZ was sampled using 286 special k points according to the linear tetrahedra method. The self-consistent calculation was performed including spin-orbit coupling at each variational step. After the band structure and the Fermi level was obtained we calculated the so-called electronic occupancy which consists of the number of occupied bands in a rectangular mesh of the BZ. This quantity was compared to $\rho_{LCW}^{ep}(\boldsymbol{k})$ defined in Eq. (1), within the approximation of a $\boldsymbol{k}$-independent overlap integral.

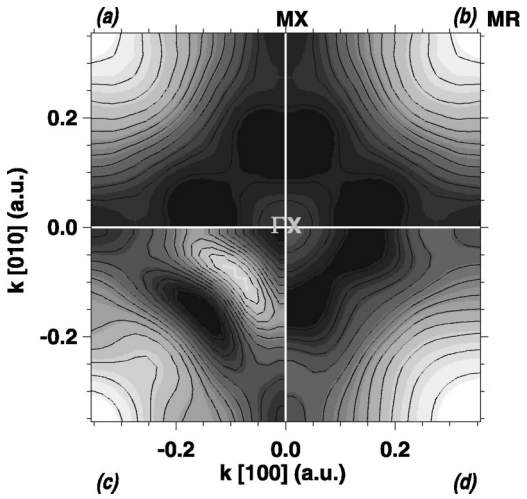

FIG. 1. Quadrants (a) and (b): 2D $\rho_{LCW}^{ep}(k_x,k_y)$ densities of $CeIn_3$ obtained from LCW folding the 2D experimental projection $\rho^{ep}(p_x,p_y)$, with p_z along the [001] axis. The contour level spacing corresponds to 0.8% of the maximum, equivalent to 14 times the statistical uncertainty of the maximum. Lower part: projected theoretical occupancies (see text). Quadrant (c) ***f***-band model, quadrant (d) ***f***-core model. 1 a.u.$=1/a_0=1.89$ Å^{-1}, where a_0 is the Bohr radius. The labeling describes the projected BZ high-symmetry points.

III. RESULTS AND DISCUSSION

The itinerancy or localization of the $4f$ electrons in heavy-fermion systems is a long debated argument. As already mentioned, the calculation of Lalic *et al.*,[6] including the f electrons in the band, could not reproduce the experimental value of magnetic moment. In fact, the observed moment is rather consistent with the expectation value of the Γ_7 duplet (0.71 μ_B) which is a possible ground state of the f multiplet (with J=5/2) in a cubic crystal field.[20] Therefore, since no moment reduction attributable to the Kondo effect is shown in $CeIn_3$, a simple picture where the f degree of freedom retains a localized, un-hybridized character (and consequently an *f*-core model) might be preferable. With this caveat, we start our discussion by comparing the electronic occupancies of the *f*-band and the *f*-core model to the experimental results. To this end, Fig. 1 shows two-dimensional line integrals of the *f*-band and *f*-core occupancies along the [001]direction [Figs. 1(c) and (d), respectively] compared to the 2D-LCW folded data of the 2D-ACAR measurement for the same projection direction (Fig. 1, upper part). The theoretical results were convoluted with a reduced experimental resolution [(0.06,0.06) a.u.] since no deconvolution procedure applied to the experimental data can restore perfectly the ''true'' data. The *f*-core model shows a fairly good agreement with the experiment in the central part of the projected

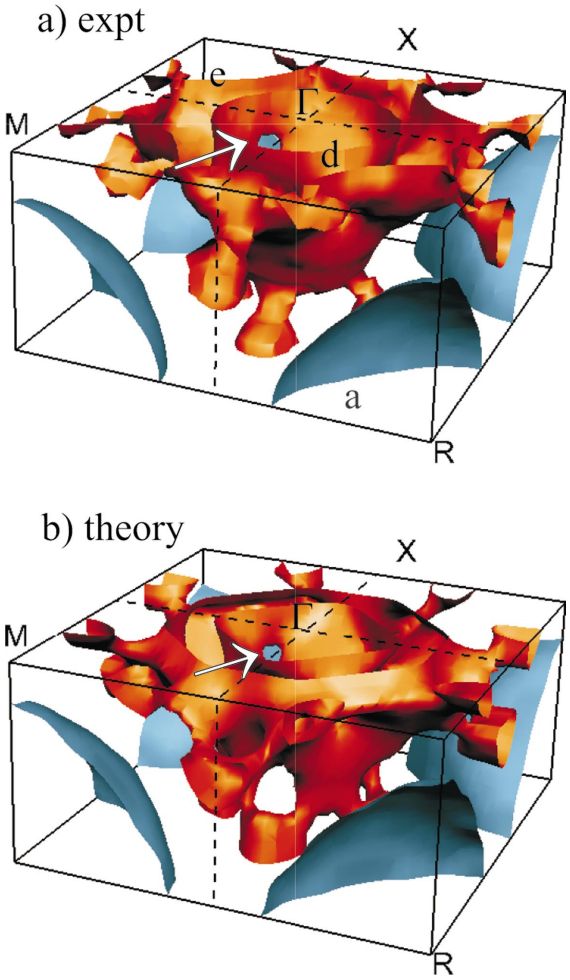

FIG. 2. (Color) **(a)** Experimental FS's for $CeIn_3$, shown in half BZ. Orange: holelike FS. The unoccupied region lies between the inner surface (d), centered at Γ, and the outer surface (e). Light blue: *R*-centered electronlike FS (a). Letters e, d, a refer also to the dHvA branches simulated in Fig. 3. **(b)** The two FS sheets (orange, blue) predicted by the *f*-core calculation. The white arrows address the necks of the holelike FS in the [111] direction described in the text.

BZ (local maximum at (0,0) and minima at (0.15,0) a.u. type) and in the shape of the highs centered at the MR points. Conversely, the complex structure of the *f*-band calculation in the central part of the BZ [maxima at (0.09,0.09) a.u. and minima at (0.15,0.15) a.u.] is almost opposite to the experimental data. Therefore, since the *f*-core calculation approximates the experimental data much better than the *f*-band one, we will refer only to the former model for further analysis of the experiment.

Although the results displayed in Fig. 1 allow us to estimate which *f* model is more realistic, the direct access to the 3D topology of the FS, which makes our experiment a rather unique tool, needs 3D reconstructed densities. The band structure, in good agreement with that calculated by Kioussis *et al.*,[8] shows that only two bands cross the Fermi level. The two resulting FS's consist of an electron like spheroidal pocket centered at the *R* points and a hole like multiply connected structure surrounding the *X* points and the Γ point.

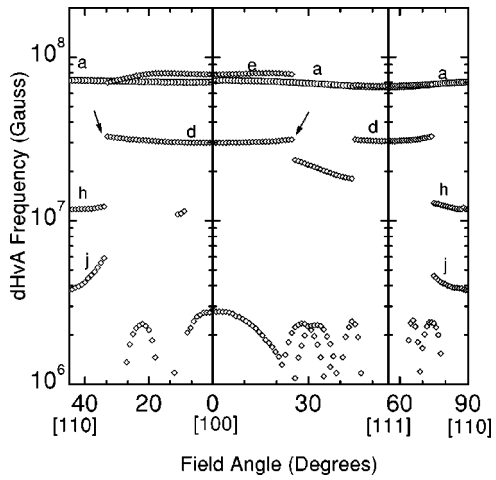

FIG. 3. Angular dependence of the dHvA frequencies pertaining to the FS sheets observed in this work. Labeling is the same as in Fig. 23 of Ref. 5.

Since, within the *f*-core model, $CeIn_3$ is a compensated metal, the two FS's enclose equal volumes. The 3D topology of the FS deduced from our experiment and predicted by the theory is shown in Fig. 2. Its upper part [Fig. 2(a)] shows (in half BZ) a 3D view of the isodensity surfaces, identified as FS's, selected at the loci of the largest amplitude variations of $\rho^{ep}_{LCW}(\boldsymbol{k})$. To select the threshold values of the LCW density we have followed the procedure described in Ref. 9. In this case two maxima, corresponding to two FS manifolds, were detected. The related Fermi volumes are $(16\pm2)\%$ and $(16\pm3)\%$ of the BZ for the *R*-centered electronlike FS (light blue) and the Γ-centered holelike FS (orange), respectively. These values are in good agreement with those obtained by the *f*-core calculation [shown in Fig. 2(b)], yielding 18% of the BZ volume for the electronlike and holelike FS's. The visual agreement between experiment and theory is striking. In particular, note the small necks of the holelike FS along the [111] direction, indicated by the white arrows, shown in both figures. The largest discrepancy between theory and experiment consists in the slightly different topology of the holelike FS (orange) nearby the *X* points. One can further test these results by simulating the angular dependence of the extremal cross sectional areas expressed as dHvA frequencies. The branches a, d, e, h, and j shown in Fig. 3 agree with those shown in Fig. no. 22 of Ref. 5 for paramagnetic $LaIn_3$. In particular, the black arrows address the existence of the necks of the holelike FS along the [111] direction discussed above.

As mentioned previously, the dHvA signals detected for $CeIn_3$ in the AF phase (Fig. 24 of Ref. 5) were quite different from those of $LaIn_3$. Of all the high-frequency branches (greater than 10^7 G) only a signal with weak angular dependence (near 2.6×10^7 G) and no discontinuities in the whole angular range of Fig. 3 remain. It is worth mentioning that, in spite of the high magnetic field required to the dHvA experiments to observe quantum oscillations in heavy fermions (typically 15 T), $CeIn_3$ retains the AF state.[21] We recall that with the type-II AF ordering (propagation vector $\boldsymbol{q}=\pi/a[111]$) the number of atoms in the unit cell is

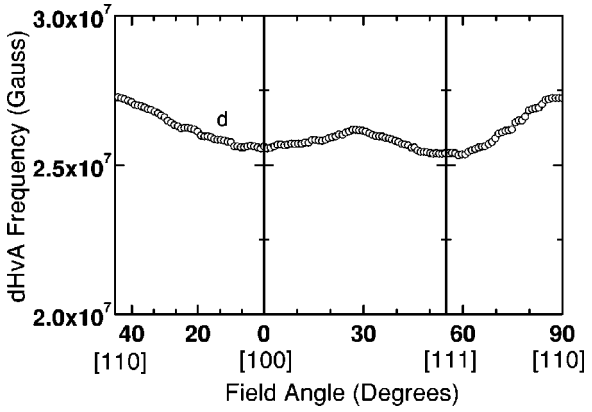

FIG. 4. Angular dependence of the dHvA signal simulated after folding the experimental $\rho^{ep}(\boldsymbol{p})$ according to the AF cell. Labeling is the same as in Fig. 24 of Ref. 5.

doubled, since the Ce atoms at position (0,0,0) and (1,1,1) are no longer equivalent. Therefore the AF periodic structure is fcc with lattice constant a_{fcc} twice the original one ($a_{fcc}=2a$). Although our measurement was in the paramagnetic phase, we folded $\rho^{ep}(\boldsymbol{p})$ according to the new cell and looked for the isodensities surfaces at the loci of the highest amplitude variations. The branch labeled as d in Fig. 4 is in good agreement with the corresponding branch shown in Fig. 24 of Ref. 5. Note beyond the absence of discontinuities, mentioned above, the slight maximum between the [100] and [111] directions which is observed in Ref. 5 as well. To understand such a close agreement between dHvA signals generated from band structures in two different phases one should realize that the FS manifold which produces branch d is relatively far from the BZ borders. Therefore it is plausible that its shape is not affected by the para-AF transition. It is well known that the main changes in the band structure caused by the AF transition consist of band gaps opening at the (new) BZ boundary. These gaps would certainly affect the electronlike *R* centered FS, whose diameter ($\simeq$0.52 a.u.) is near the distance between the hexagonal planes of the AF BZ (0.61 a.u.). Moreover, due to the folding, the FS sheets labeled as a and e in Fig. 2(a) interfere, causing the high-frequency signals to disappear. Further overlaps of the FS manifolds should be the reason of the changes in branch d, from the paramagnetic phase (Fig. 3) to the AF phase, observed in Fig. 24 of Ref. 5 and confirmed by our simulation, deduced from the paramagnetic phase (Fig. 4). It should be clear that our simulation and the consequent interpretation of the dHvA frequencies observed for $CeIn_3$ is valid only if the magnetic structure of AF $CeIn_3$ is fcc. Indeed, of all the RE-In_3 compounds, $CeIn_3$, which displays the largest differences in frequency branches with respect to those observed in $LaIn_3$, is the only one to show a type-II (fcc) magnetic structure. Our analysis shows that these differences can be understood without the need to invoke the itinerancy of the $4f$ electrons in $CeIn_3$. Conversely, we propose that the $4f$ electrons retain a localized character in the AF and heavy fermion state. In a way, this evidence indicates that the *f* electrons should not contribute directly to s.c. Obviously, the question of which electrons participate in the formation of the Cooper pairs is essential to elucidate the s.c. mechanism in this class of materials. For example, in the case of the ferromagnetic system UGe_2, Shick *et al.* propose that the s.c. is originated by *p*-wave-type (triplet) pairing of electron spins associated with *itinerant* $5f$ electrons.[22] However, contrary to their hypothesis, our measurements in the paramagnetic and in the ferromagnetic phases indicate that the $5f$ electrons of UGe_2 are mostly localized.[23] This kind of behavior is typical of several magnetically ordered heavy fermions, where the expected wash out of the $4f$ (or $5f$) electron magnetic moments below the Kondo temperature as a result of the hybridization between *f* electrons and conduction electrons is *not* observed (see, for example, CeB_6, $CePd_2Al_3$, UPd_2Al_3, CePdAl, CeSb). In these cases, it was proposed that a mechanism analogous to the electron-phonon-type enhancement in ordinary metals, provided by the electron-magnon interaction, could account for the mass enhancements of the conduction electrons.[24] We conjecture that the latter mechanism is responsible for the electron pairing that leads to the s.c. In other words, the indirect exchange interaction between the *localized f* electrons, which is transmitted via the polarization of the conduction electrons, could provide the pairing mechanism in an analogous manner to that provided by the phonon-conduction electrons interaction in standard BCS superconductors. This possibility is consistent with the narrow region of pressure (around p_c) where s.c. is confined. Indeed, by increasing the pressure above p_c the interaction between the $4f$ electrons should lose its indirect character and therefore the ability to pair the conduction electrons. A somewhat similar mechanism has been proposed in Ref. 25 for the heavy-fermion antiferromagnet UPd_2Al_3, where s.c. is obtained without application of high pressure. For this system it was suggested that at least two $5f$ electrons are localized in the U^{4+} state, while the remaining $5f$ electron is itinerant due to a larger hybridization with the conduction electrons.[25] The authors propose that the magnetic excitations resulting from the exchange interactions between the magnetic moments produce the pairing interactions between the itinerant electrons which cause superconductivity.

In conclusion, we have shown an unprecedented comparison, on a pixel by pixel base, between theory and experiments of the multisheet FS of $CeIn_3$ in the paramagnetic phase. Moreover, our simulation of the dHvA signals suggests the persistence of an indirect interaction, RKKY-like, between localized *f* electrons up to the onset of the s.c. transition. This magnetic interaction appears to be a valid candidate for the pairing of the conduction electrons which give rise to s.c.

ACKNOWLEDGMENTS

We wish to thank G. Kontrym-Sznajd and J. Rusz for their contribution to this work.

*Corresponding author. Also at Istituto Nazionale di Fisica della Materia, Corso Perrone 24, 16152 Genova, Italy. Email address: Biasini@bologna.enea.it

[1] F.M. Grosche, I.R. Walker, S.R. Julian, N.D. Mathur, D.M. Freye, M.J. Steiner, and G.G. Lonzarich, J. Phys.: Condens. Matter **13**, 2845 (2001), and references therein.

[2] H. v. Löhneysen, C. Pfleiderer, T. Pietrus, O. Stockert, and B. Will, Phys. Rev. B **63**, 134411 (2001).

[3] K. Satoh, I. Umehara, N. Nagai, Y. Onuki, I. Sakamoto, M. Hunt, P. Meeson, P.A. Probst, and M. Springford, J. Magn. Magn. Mater. **104-107**, 1411 (1992).

[4] Y. Kurosawa, I. Umehara, M. Kikuchi, N. Nagai, K. Satoh, and Y. Onuki, J. Phys. Soc. Jpn. **59**, 1545 (1990).

[5] Y. Onuki and A. Hasegawa, *Handbook on Phys. and Chem. of Rare Earth* (1995), Vol. 20, Chap. 135.

[6] M.V. Lalic, J. Mestnik-Filho, A.W. Carbonari, R.N. Saxena, and H. Haas, Phys. Rev. B **65**, 054405 (2001).

[7] J.M. Lawrence and M. Shapiro, Phys. Rev. B **22**, 4379 (1980).

[8] N. Kioussis, J. Thevenot, B.R. Cooper, and Q.G. Sheng, J. Appl. Phys. **79**, 6420 (1996).

[9] M. Biasini, G. Ferro, G. Kontrym-Sznajd, and A. Czopnik, Phys. Rev. B **66**, 075126 (2002).

[10] M. Biasini, G. Kontrym-Sznajd, M.A. Monge, M. Gemmi, A. Czopnik, and A. Jura, Phys. Rev. Lett. **86**, 4612 (2001).

[11] S.B. Dugdale, H.M. Fretwell, M.A. Alam, G. Kontrym-Sznajd, R.N. West, and S. Baldrzadeh, Phys. Rev. Lett. **79**, 941 (1997).

[12] S. Berko, *Proceedings of the International School of Physics "Enrico Fermi" Course*, edited by W. Brandt and A. Dupasquier (North-Holland, Amsterdam, Course LXXXIII, 1983), p. 64.

[13] D.G. Lock, V.H. Crisp, and R.N. West, J. Phys. F: Met. Phys. **3**, 561 (1973).

[14] J.H. Kaiser, R.N. West, and N. Shiotani, J. Phys. F: Met. Phys. **16**, 1307 (1986).

[15] A. Rubaszek, Z. Szotek, and W.M. Temmermann, Phys. Rev. B **63**, 165115 (2001).

[16] P. Blaha, K. Schwartz, and J. Luitz, *WIEN97*: A Full Potential Linearized Augmented Plane Wave Package for Calculating Crystal Properties (Tech. Universität Wien, Austria, 1999), ISBN 3-9501031-0-4.

[17] M. Biasini, G. Ferro, M. Monge, G. di Francia, and V. La Ferrara, J. Phys.: Condens. Matter **12**, 5961 (2000).

[18] A.M. Cormack, J. Appl. Phys. **35**, 2908 (1964).

[19] G. Kontrym-Sznajd and E. Jozefczuk, Mater. Sci. Forum **255-257**, 754 (1997).

[20] K.R. Lea, M.J.M. Leask, and W.P. Wolf, J. Phys. Chem. Solids **23**, 1381 (1962).

[21] See Ref. 5 p. 43, line 14.

[22] A.B. Shick and W.E. Pickett, Phys. Rev. Lett. **86**, 300 (2001).

[23] M. Biasini and R. Troc, submitted to Phys. Rev. B.

[24] T. Kasuya, O. Sakai, H. Harima, and M. Ikeda, J. Magn. Magn. Mater. **76&77**, 46 (1988).

[25] N.K. Sato, N. Aso, K. Miyake, R. Shiina, P. Thalmeier, G. Varelogiannis, C. Geibel, F. Stedlich, P. Fulde, and T. Komatsubara, Nature (London) **410**, 340 (2001).